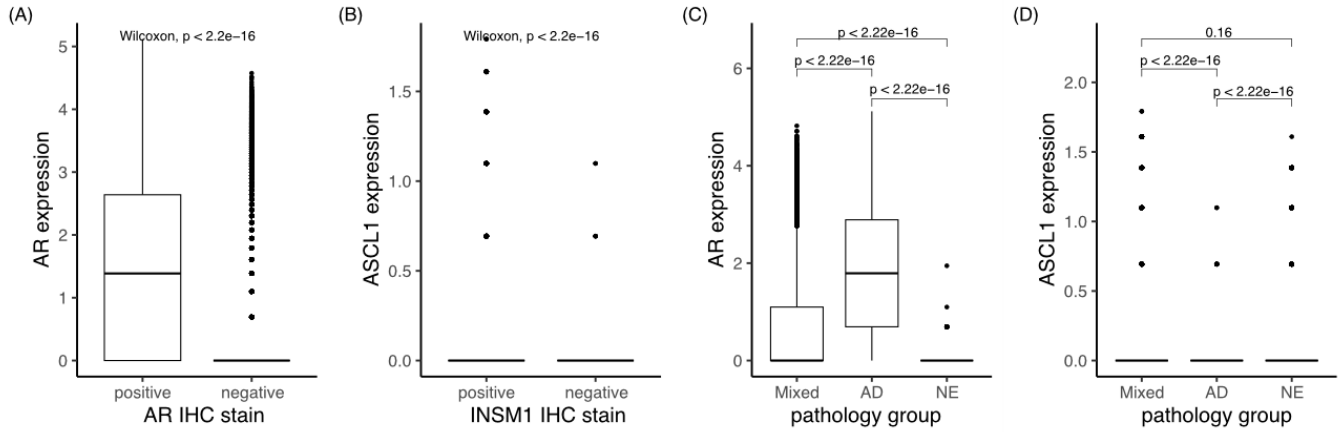

Fig. S1: AR and ASCL1 gene expression in histology and pathology groups.

(A) AR expression is significant higher in samples with positive AR IHC stain. There is little but not no expression of AR in the samples with no AR staining.

(B) ASCL1 expression is significantly higher in samples with positive INSM1 IHC stain.

(C) AR expression is highest in AD tumours, followed by Mixed then NE tumours.

(D) ASCL1 expression is comparable between AD and NE tumours while rare in AD ones.

The statistical test used was Wilcoxon rank test.

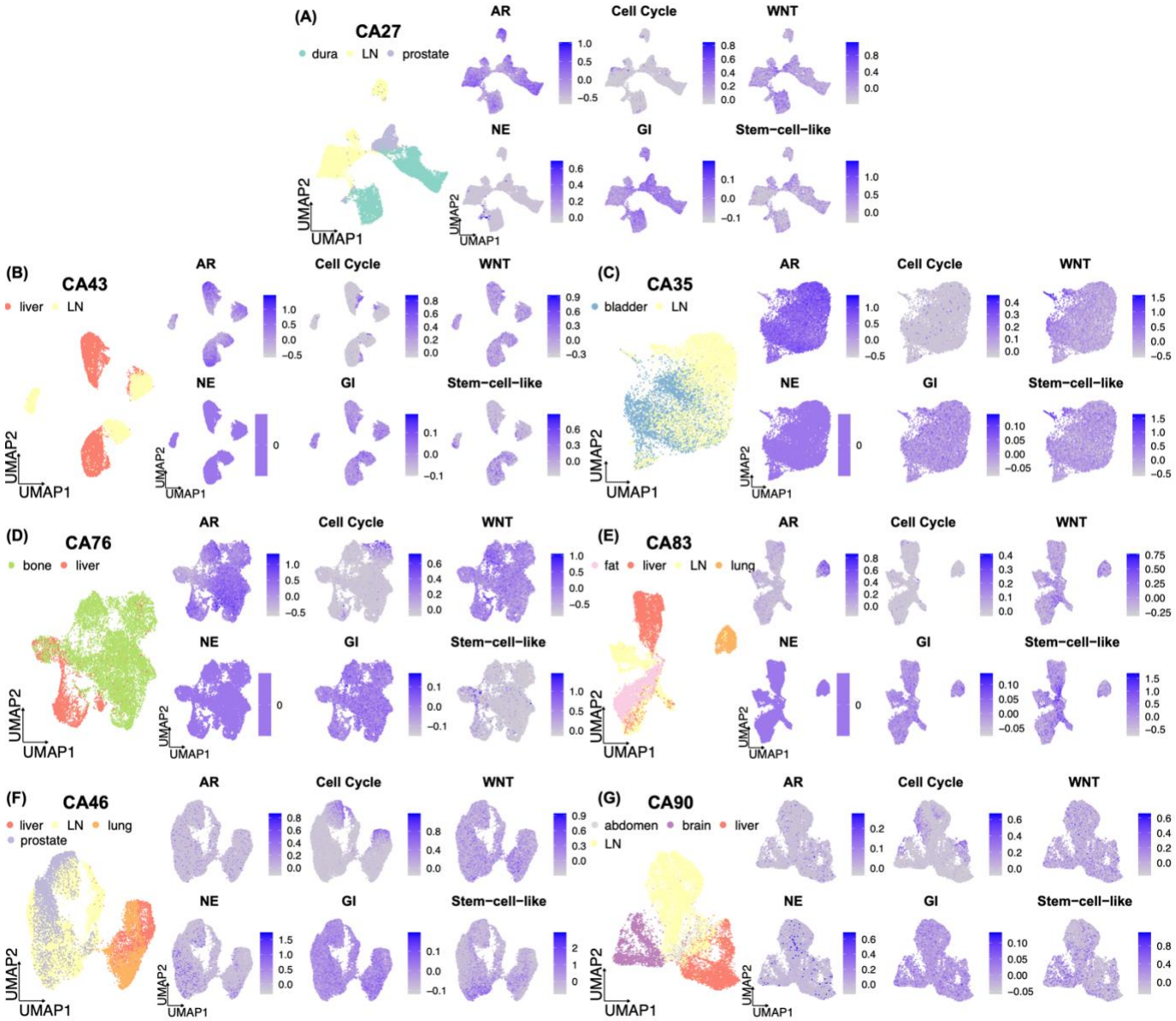

Fig. S2: Expression of AR related, NE phenotype, cell cycle, GI, WNT subtype, and stem-cell-like subtype in tumour cells across all lesions of individuals.

(A-G) Signature expression in CA27, CA43, CA35, CA76, CA83, CA46 tumours, respectively. The genes belonging to each signature is presented in Supplementary Table S2. Limited inter-lesion heterogeneity was shown by the six signatures. Expression of signatures was uniform except proliferating tumour cells clustered. Importantly, the cell populations with low AR or NE signatures were not further explained by the rest signatures, showing no distinguishment between CA83 lung and other CA83 tumours in E. The NE signature has zero expression in all AD samples, little in Mixed samples and more in NE samples while interestingly, AR signature expression was found in NE tumours.

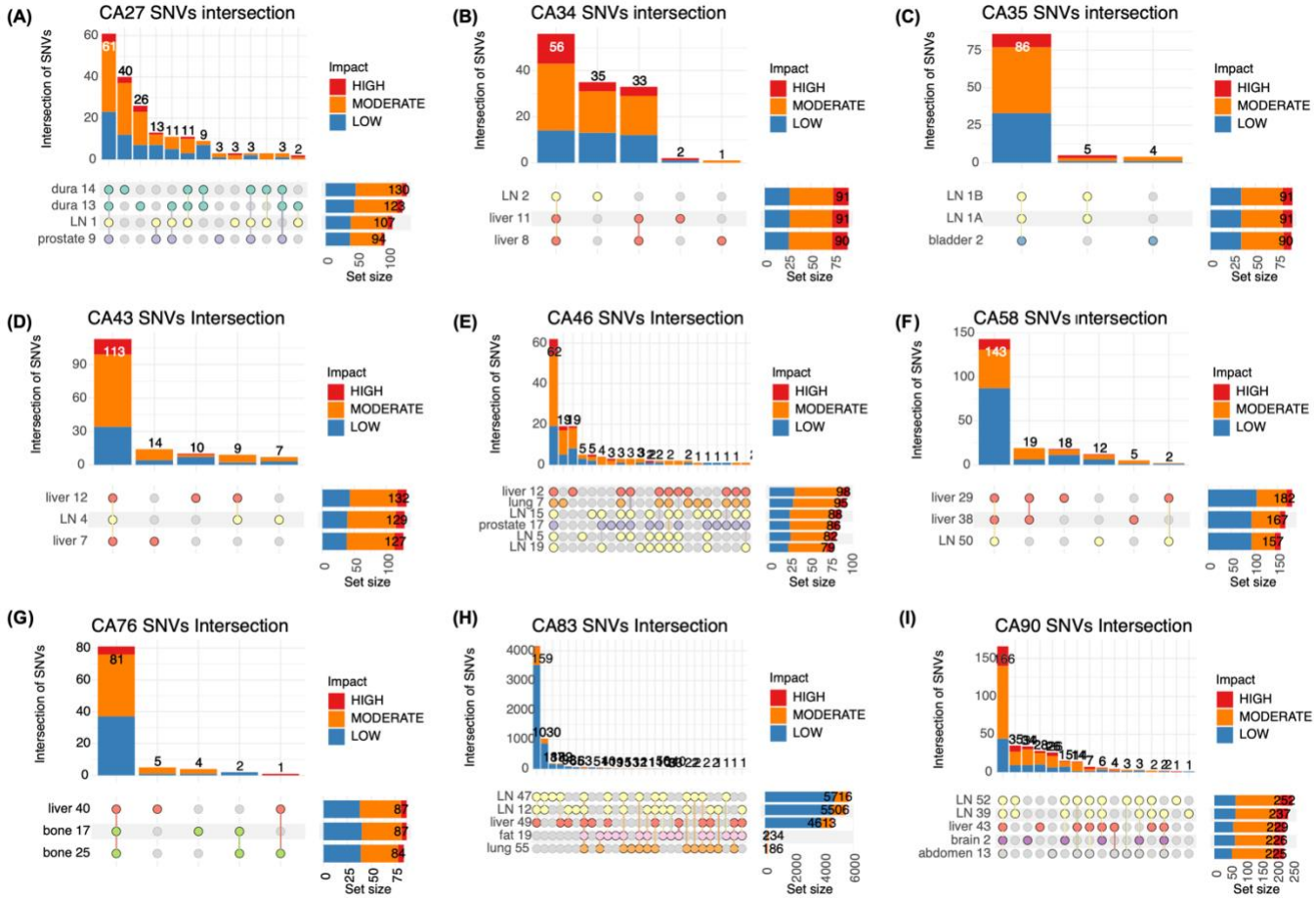

Fig. S3: UpSet plots showing the SNVs intersection between lesions of individuals.
(A-I) UpSet plots of all patients. Little genetic inter-lesion heterogeneity was observed as most SNVs were shared between all samples within patients, similar number of SNVs were called among lesions and a similar proportion of SNV impacts were identified, with the only exception being the fat and lung samples of CA83. The height of the bar represents the number SNVs overlapped between samples linked in the below panel. The colours of the bar are split by impacts annotated by VEP. Besides SNVs shared by all lesions, tumours from the same organ were more likely to share SNVs.

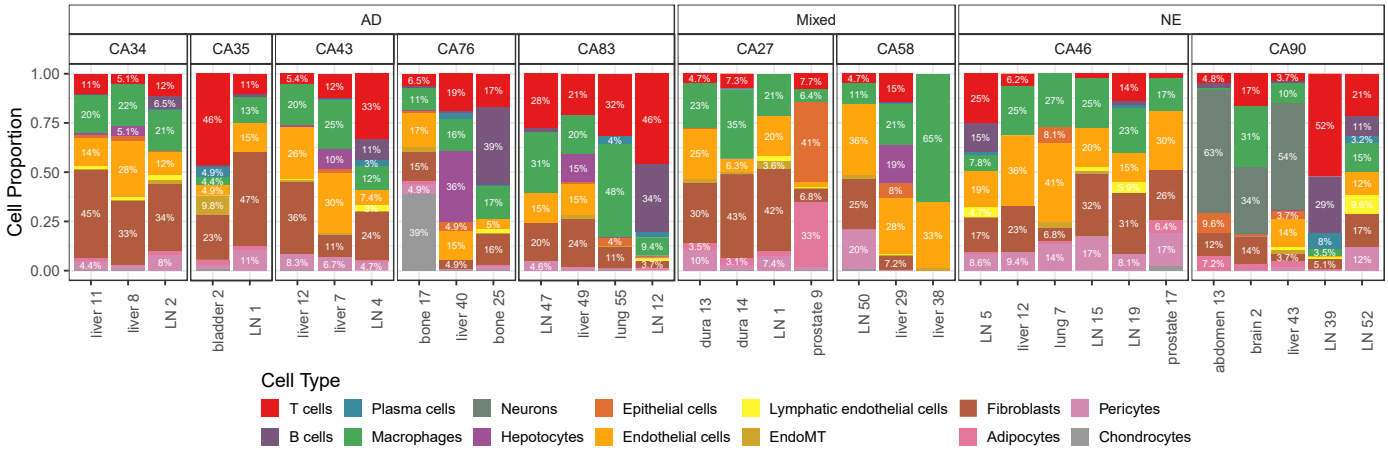

Fig. S4: Non-tumour cell composition across samples. The normal cell composition varied across samples and patients, with some association with organ and pathology class (Fig. 3F). Neuron cells were exclusively found in CA90 samples, except the lymph nodes.

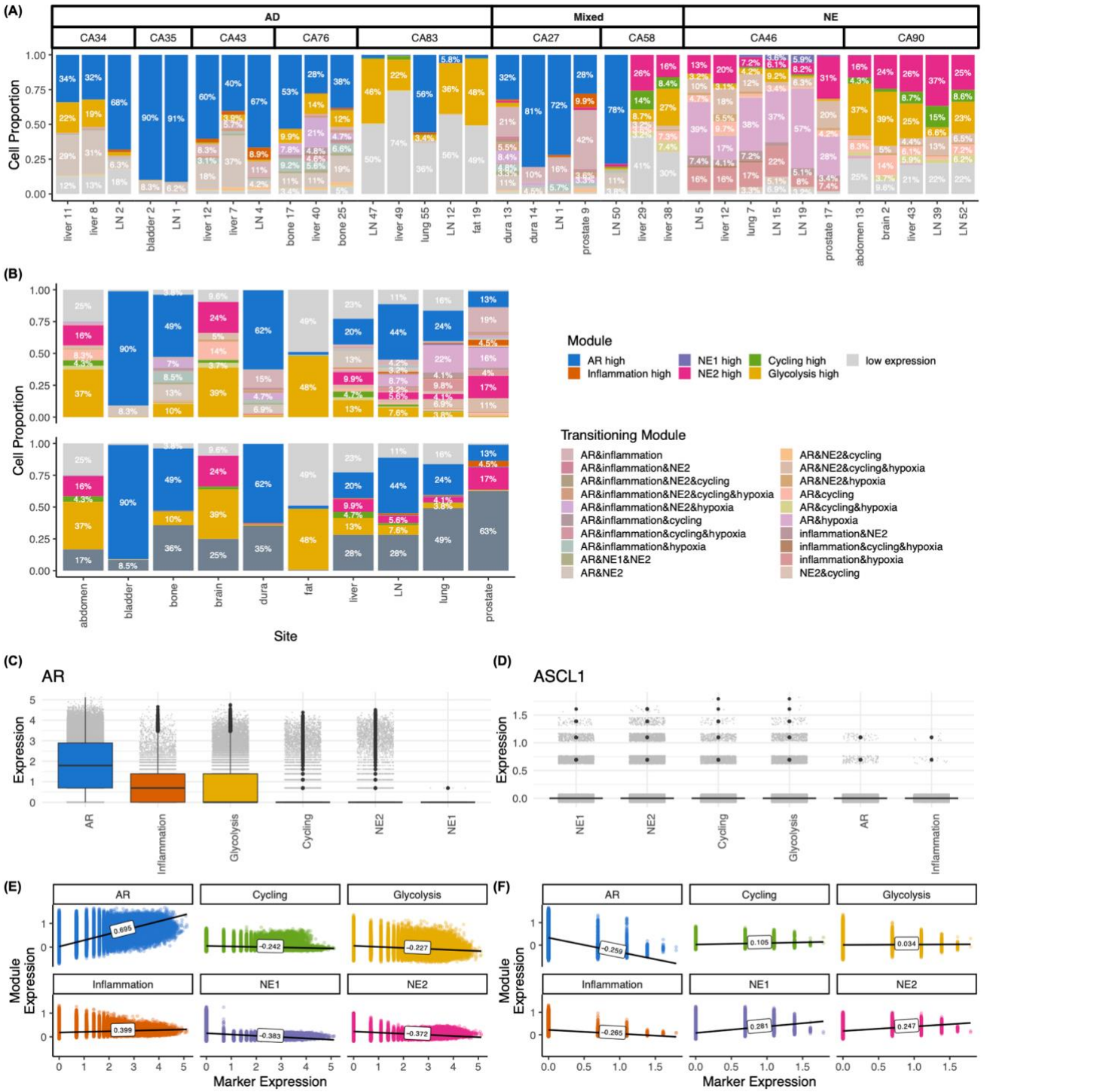

Fig. S5: Composition of archetype modules across samples and sites, and association with *AR* and *ASCL1* gene expression.

(A) Composition of archetype modules across samples. The legends are the same as in panel B.

(B) Composition of archetype modules across organs. There was no organ specific pattern of module composition in cells with an absolute module annotation (top) or in a transition state (bottom).

(C-D) Expression AR and ASCL1 in cells based on their module annotation. Modules were ranked based on gene expression level. The *AR* gene has the highest expression in cells annotated as belonging to the AR module group, followed by those annotated as being from the Inflammation and Glycolysis module groups. *ASCL1* has highest expression in cells of the NE1 Module, and lower in those of the NE2 and Cycling Module. The Spearman correlation adjusted p values are less than 10^{-16}.

(E) Spearman correlation between module signatures expression and expression of *AR*. *AR* is most positively correlated with AR Module expression, followed by the Inflammation Module, and is negatively correlated with the rest modules.

(F) Spearman correlation between module signatures expression and expression of *ASCL1*. NE1 is more correlated with *ASCL1* expression than NE2. The Spearman correlation adjusted p values are less than 10^{-16}, except the p value between Module 6 and ASCL1 expression is 9.8×10^{-44}.

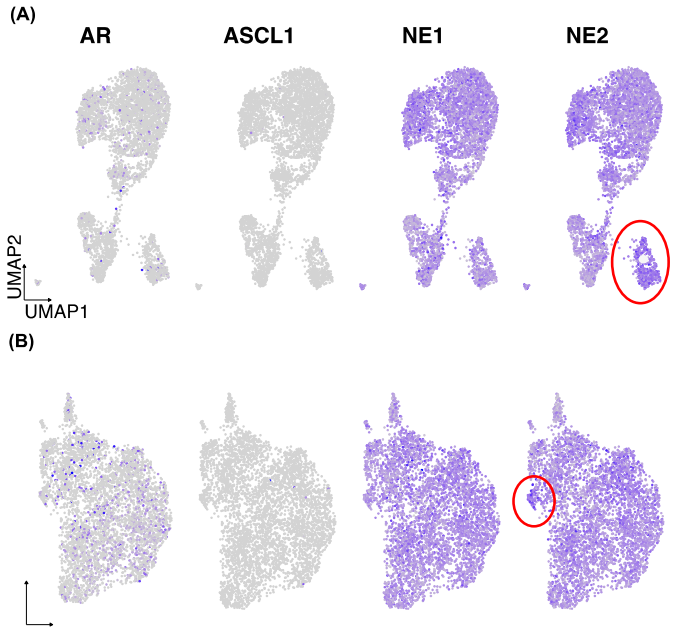

Fig. S6: Expression of NE1 and NE2 signatures in tumour cells of CA90 primary tumours.

(A) Expression of AR, ASCL1, NE1 and NE2 signatures in tumour only cells of CA90 primary prostate tumour site 13.NE2 expression was higher in the right small cluster than in the rest of the cells.

(B) Expression of AR, ASCL1, NE1 and NE2 signatures in tumour only cells of CA90 primary prostate tumour site 18, showing homogenous expression of NE1 and NE2 signatures.

Tumour cells were separated from normal cells through SingleR annotations.

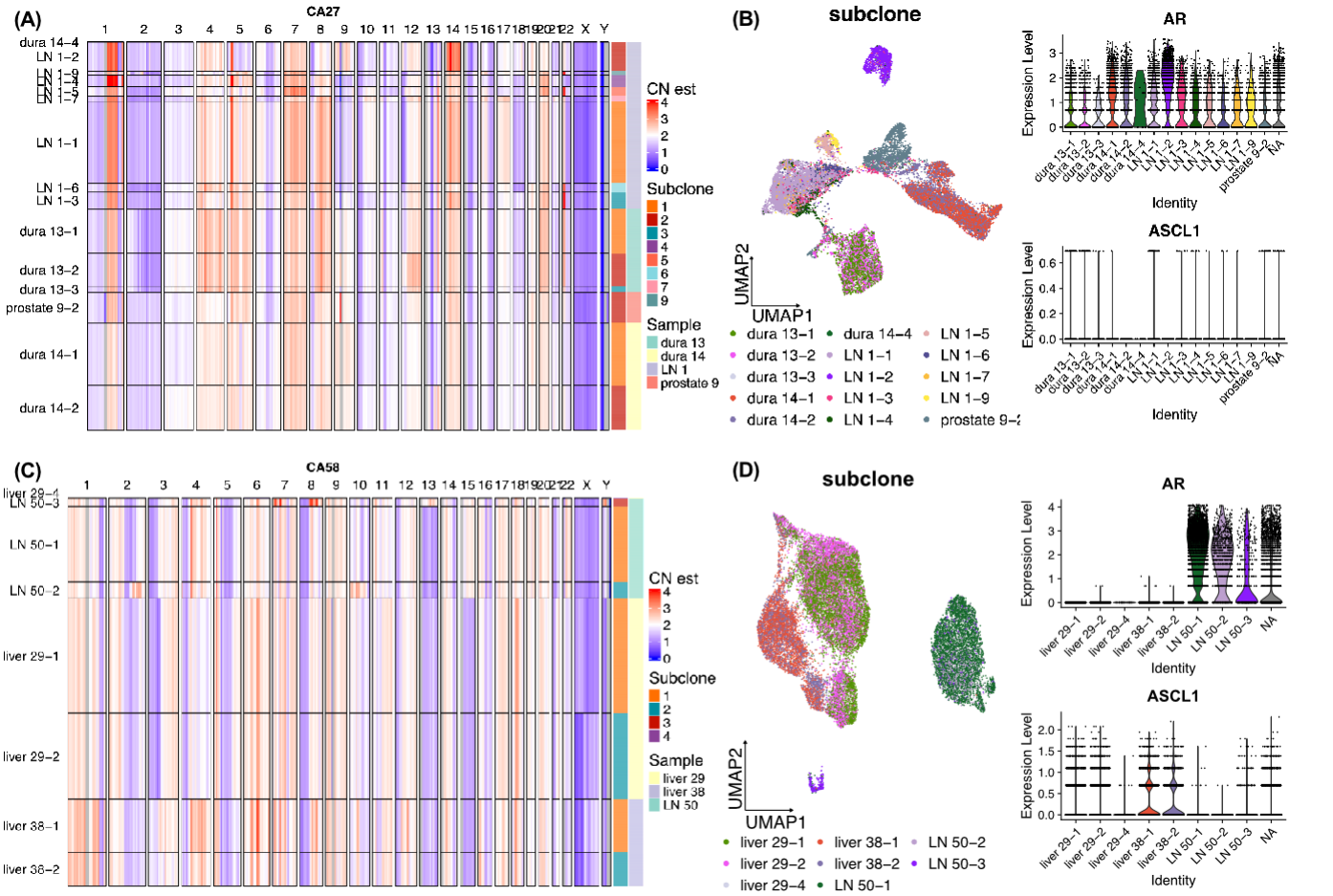

Fig. S7: Subclone overview for CA27 and CA58 with AR and ASCL1 expression.

(A) Joint subclones inferred by ATAClone for all lesions of CA27. The subclones shared most background CNVs originated from the same ancestor. The evolutionary relationship of metastases was not linear, with subclones in the different metastases not being direct daughters of one another. The LN sample has the greatest number of subclones and distinct amplifications.

(B) UMAP of tumour cells of CA27 with expression of *AR* and *ASCL1* grouped by subclones. All the subclones have comparable *AR* expression. *ASCL1* expression is also shared across subclones, suggesting the emergence of NE subpopulations was spontaneous across subclones. Inter-lesion clusters are mostly, but not always, dominated by one subclone.

(C) Joint subclones inferred by ATAClone for all lesions of CA58. Livers and LN 50 subclone 3 cells have more CNV than the rest subclones. Although the liver samples have NE signatures, they are distinct clones. The LN 50 subclone 3 is the most distinct subclone.

(D) UMAP of integrated tumour cells of CA58 with expression of *AR* and *ASCL1* grouped by subclones. There is a cluster in NE cells in the LN sample, which all belong to subclone 3. This subclone has both *AR*+ and *ASCL1*+ cells. Their CNV profile is more similar to the other subclones of LN 50 rather than the liver clones, indicating that emergence of NE features in this subclone was separate to the emergence of NE in the liver samples.

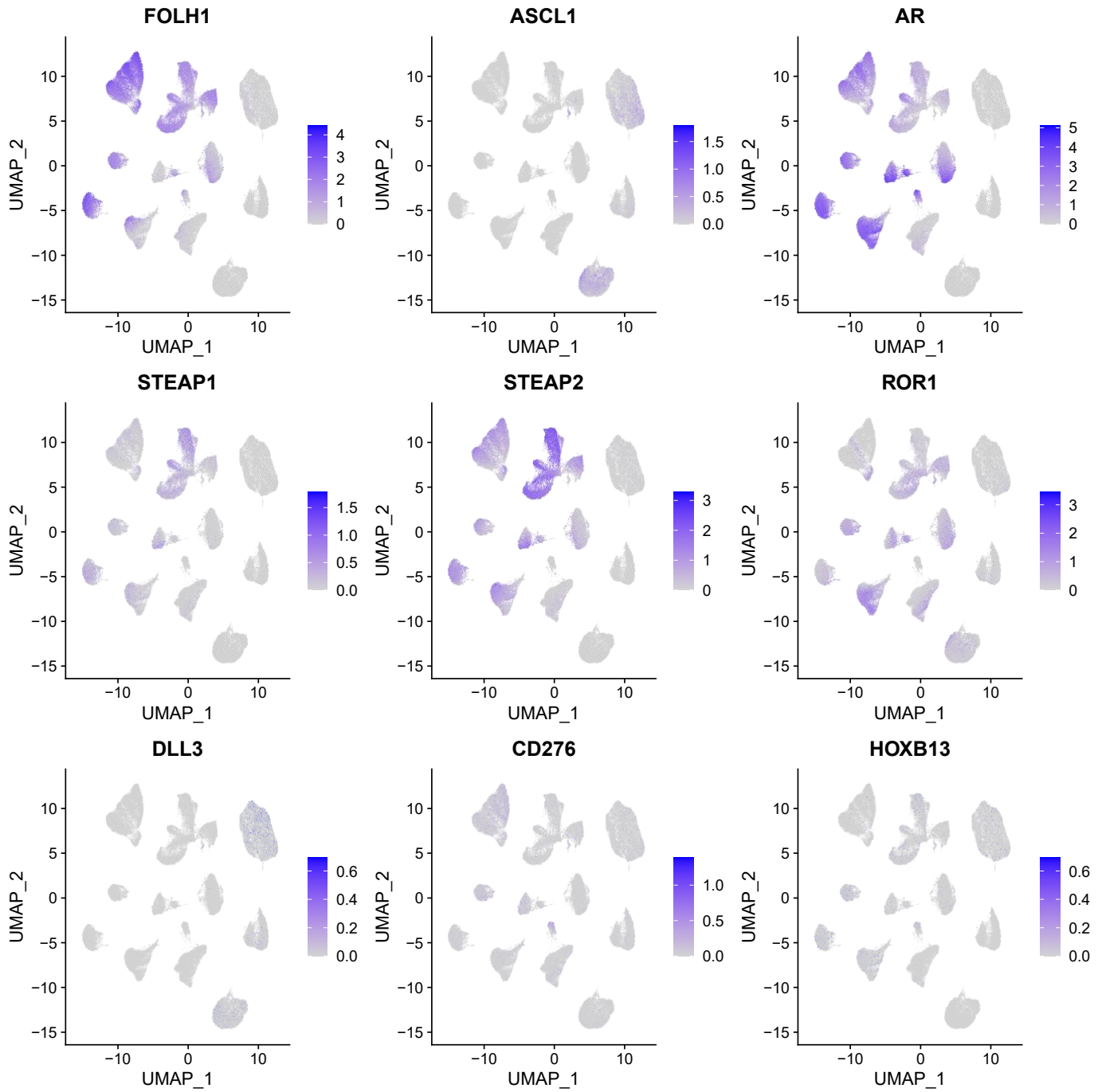

Fig. S8: Expression of therapeutic targets including *FOLH1*, *STEAP1/2*, *ROR1*, *DLL3*, *CD276*, *HOXB13* and mCRPC phenotypic markers (*AR* and *ASCL1*) across tumour cells in our cohort. *FOLH1* had the strongest expression, followed by *STEAP2* and *STEAP1*. *STEAP2/1* had high expression in ARlow samples (e.g. CA27), which have the most consistent expression to *FOLH1*. *ROR1* had limited expression except CA76 samples with low *FOLH1* expression. *CD276* and *HOXB13* had very weak expression across cells with their relation to *FOLH1* expression remains unclear in this cohort. *DLL3*, a potential NE marker, had a sparse low expression in NE samples. Except *CD276* and *HOXB13* with barely any expression, *STEAP1/2* had a largest potential to be complementary to *FOLH1* therapeutic range while *DLL3* could target *FOLH1* negative populations (NE samples).

Supplementary Note 1
Identifying and subtyping non-tumour cells

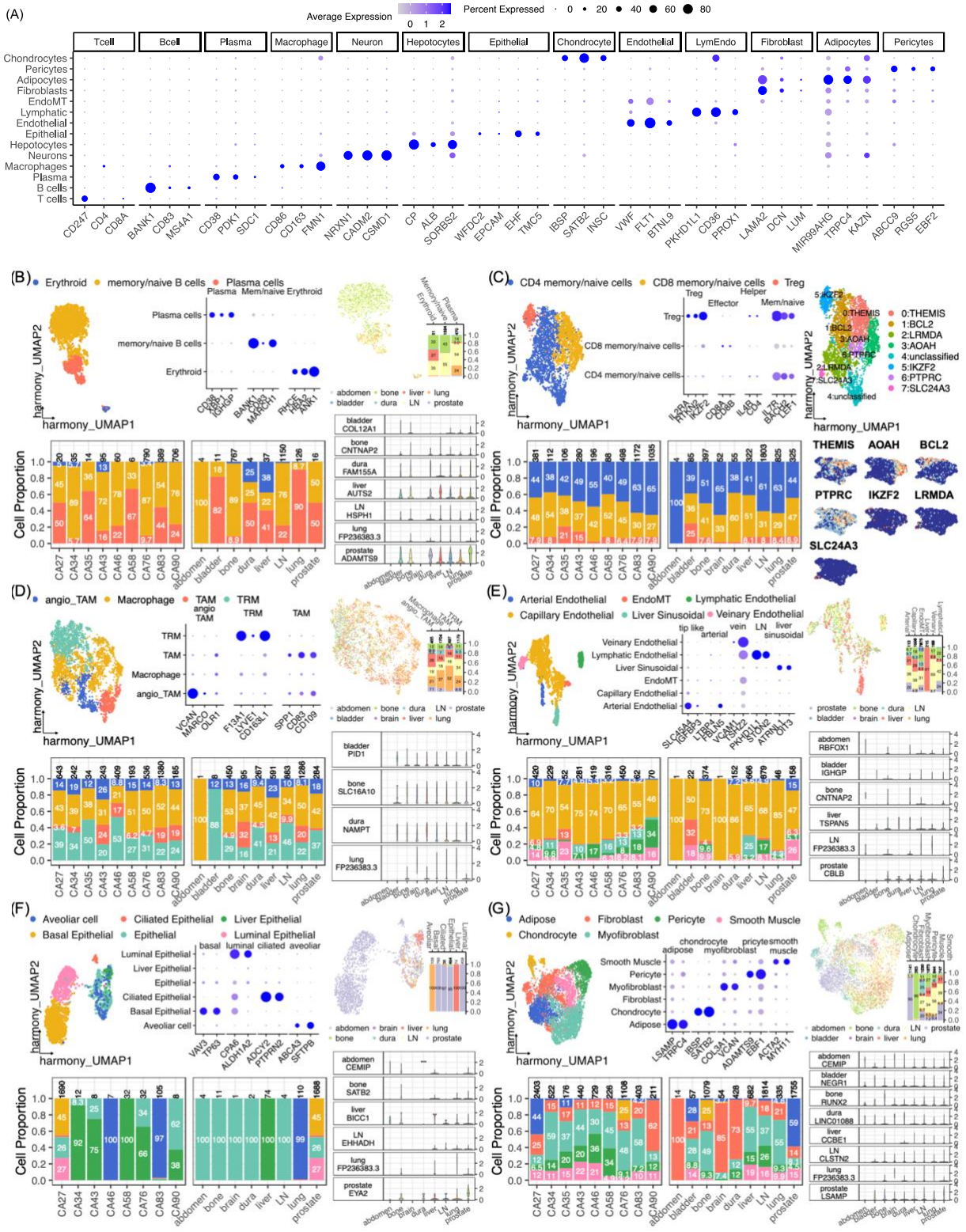

There were in total 36,108 normal cells across all our samples, which included immune populations, such as T cells, B cells, plasma cells, and macrophages, stromal populations, such as fibroblasts, adipocytes, endothelial cells and pericytes, as well as epithelial cells and neurons, and organ-specific normal cells such as hepatocytes, chondrocytes (Fig. 3E).

The cell types were identified through typical markers explained in next sections and shown in (A). B cells were characterized by *MS4A1* (CD20), *CD83* expression and *BANK1* which involves in B cell signalling pathway[1,2]. T cells remained poorly differentiated as there was a weak signal from the cytotoxic marker *CD8A* and the CD4+ T cell marker *CD4,* but there was overexpression of *CD247*[3]. We also identified macrophage cells based on the expression of *CD86*, *CD163* and *FMN1*. The proportion of T cells and B cells was concordant with the cell proportion estimate from

histological staining with CD3, CD8 and CD20 but a non-significant correlation was found between the proportion of macrophages and CD68 stain intensity (Supplementary Note 4).

We also identified large clusters of cells expressing typical fibroblast markers *DCN*, *LUM*, and *LAMA2*. Collagen genes were largely expressed in fibroblasts but also in other fibroblast-like cells such as adipocytes and pericytes[4,5] (A). Adipocytes were characterized by having a high expression of *LAMA2*, *MIR99AHG*, *TRPC4* and *KAZN,* while pericytes upregulated *ABCC9*, *RGS5* and *EBF2* instead. *VWF* was used to annotate endothelial cells and the expression of *BTNL9* and *FLT1* highlighted the vascular endothelial growth and angiogenesis associated with tumour growth[6–8]. Lymphatic endothelial cells had specific marker expression (*PKHD1L1*, *CD36*, *PROX1*) and separated from common endothelial cells (A).

Hepatocytes showed distinct typical signatures like *CP*, *ALB* and *SORBS2* (A). Neurons were enriched with astrocytes makers such as *NRXN1*, and also genes associated with neuron development (*CSMD1*), and excitatory signaling (*CADM2*) [9–12]. Epithelial cells were identified as expressing with *WFDC2* and *EPCAM* but also upregulated cancer-associated genes like *EHF*, *TMC5* [13,14]. Chondrocytes, or osteoblasts, if considering the source of this cell type was bone, upregulated *IBS, P SATB2* and *INSC* (A).

To dive deeper into the functional status and immune subtypes, we extracted and re-analysed each immune population separately (B-D). As B cells primarily expressed naïve and memory markers like *BANK1*, *CD83*, and *MARCH1*, subclustering did not enable the identification of cell subtypes other than plasma cells (B) [2,15]. T cells also overexpressed naïve markers, and fully differentiated CD4 and CD8 T cells were not revealed by subclustering, but regulatory T cells with markers *IL2RA*, *RTKN2*, and *IKZF2* were identified and mostly found in CA83 and CA90[3,16] (C). Although lack of canonical T cell subtypes, DEA between T cells subclusters found signatures linked with defective immune response and immune-suppressive behaviour like *THEMIS* and *BCL2* [17,18] (C). Tumour-associated macrophages (TAM), with markers *SPP1*, *CD83* and *CD109* and even a small group of cells with additional angiogenesis markers like *VCAN*, dominated the macrophage population (D). The rest of cells were either tissue-resident macrophages (TRM) (*F13A1*, *LYVE1* and *CD163L1*) or macrophages with no clear subtype markers[19]. The majority of macrophages were found in CA83 (36%) and mostly in lung samples (33%) (D).

We followed a similar procedure with stromal cells, and, contrary to immune populations, we identified organ-specific subtypes and distribution (E-G). For endothelia cells, liver and LN had specific endothelial cell types while artery endothelial cells were found to be enriched in LN and bone, suggesting a role on immune modulation with active angiogenesis (E). Epithelial cells in the dataset primarily belonged to the prostate of CA27 sample. We identified a number of epithelial subtypes, including basal (*VAV3*, *TP63*), luminal (*CPA6*, *ALDH1A2*) and ciliated (*ADCY2*, *PTPRN2*) subtypes[20] (F). Organ specific epithelial cells, although a small population, were also found in liver and lung as liver epithelial cells (*BICC2*, *GLIS3*, *CTNND2*) and alveolar epithelial cells (*ABCA3*, *SFTPB*), respectively (F). The cluster of fibroblast cells was the largest stromal cell population, and included several subtypes, including adipose, chondrocytes, pericytes, myofibroblasts and smooth cells. Except adipocytes (*LSAMP*, *TRPC4*) and chondrocytes (*IBSP*, *SATB2*), which were primarily in CA27 prostate and CA76 bone, other subtypes such as pericytes (*ADAMTS9*, *EBF1*), myofibroblasts (*COL3A*, *VCAN*), and smooth muscle (*ACTA2*, *MYH1*) were seen mostly seen in liver and LN (F) [4,5,21]

Supplementary Note 2
NE1 and NE2 dissect NE phenotype plasticity

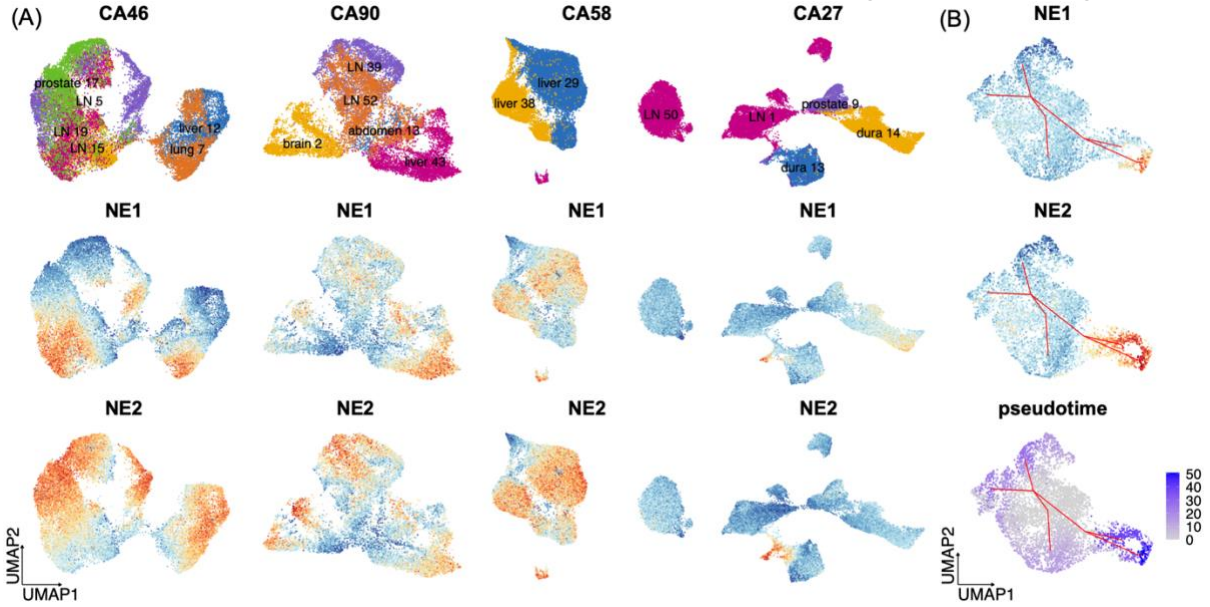

We aimed to investigate whether the NE1 and NE2 Modules represented different stages of NE development. There was high expression of both NE1 and NE2 Modules in purely NE samples such as lesions from CA46 and CA90 and liver lesions from CA58 (A). However, there were marked differences in the patterns of expression within each lesion, with solely high expression of NE1 or 2 ($NE1^{high}$ or $NE2^{high}$), or a combination in a subset of cells (NE^{mixed}). We therefore hypothesized that NE1 might represent a more differentiated NE state better correlated with *ASCL1*, while NE2 might represent a transitory, plastic state from adenocarcinoma. We checked the expression of the signatures in primary tumours of CA90 prostate and found positive expression of NE1 and NE2 Modules in the low AR and ASCL1 negative context (Fig. S6). Here, the NE2 Module showed specifically higher expression in a small group of cells which could be undergoing a transition process similar to CA27 (A).

To dissect this, we investigated the lesions from CA27, as all lesions had a combination of both phenotypes. We first focused on the CA27 dura 13 sample since the development of NE phenotype from amphicrine cells was free from subclone evolution in this sample (B). To capture the developmental expression trajectory from adenocarcinoma cells to NE cells, we performed pseudotime analyses and estimated the trajectory paths between archetype module cells, using the AR module cells as the starting point. Cells were divided into $NE2^{high}$, NE^{mixed} and $NE1^{high}$ groups. We found that NE2 had a high expression level in a larger cell population than the NE1 signature (B). Pseudotime analyses identified that NE^{mixed} cells showed the furthest distance from the AR module, suggesting a more matured state when there was co-expression of both signatures (Fig. 4D). In contrast, $NE2^{high}$ cells were positioned between the AR module and NE^{mixed} cells while $NE1^{high}$ cells were rare in this sample, considering its expression in other NE samples in patients with clinical diagnosed NE like CA46 and CA90. Overall, NE1 and NE2 signatures indicate different NE states.

Supplementary Note 3
Evaluation of NE1 and NE2 signatures in external and pre-clinical public data sets

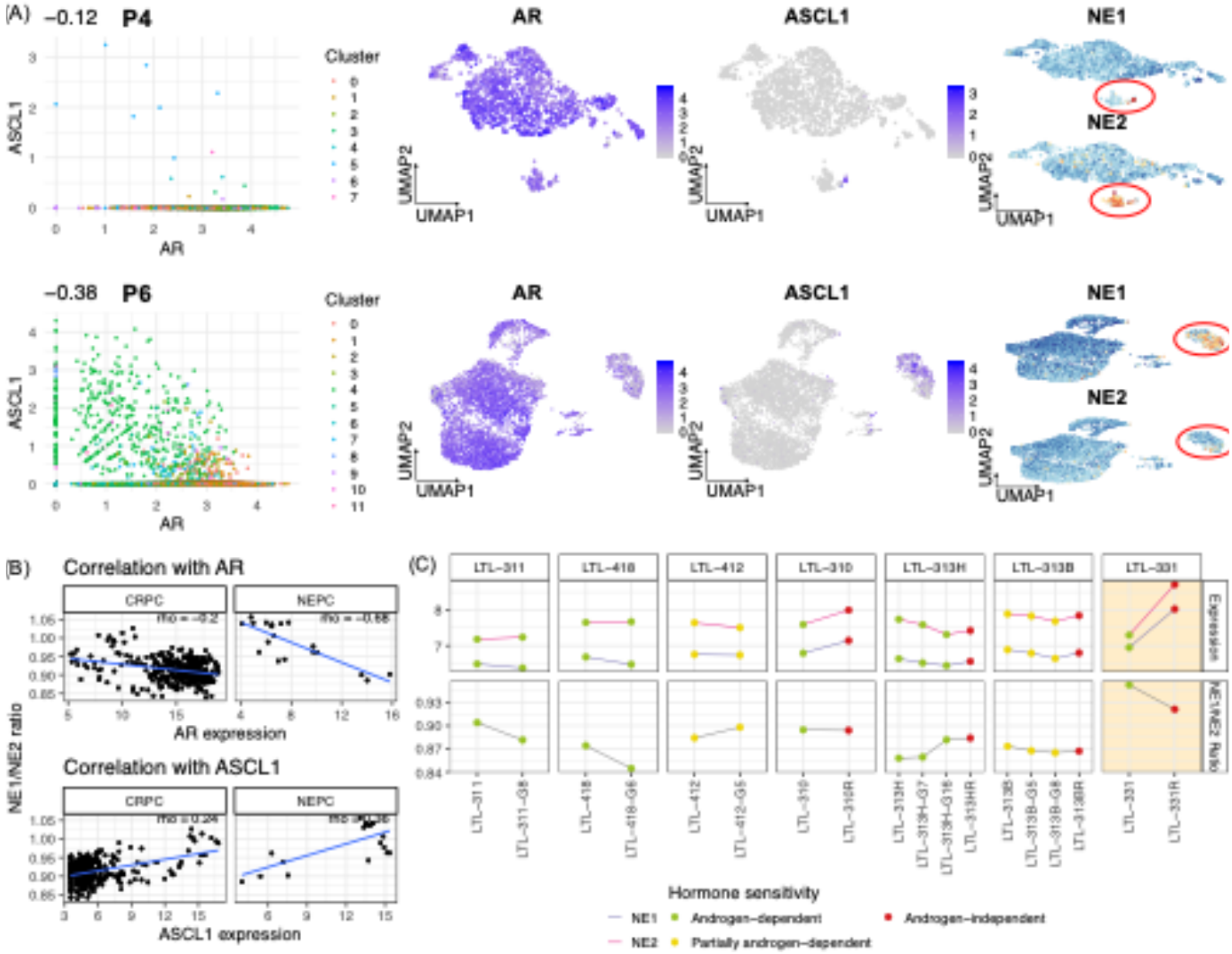

We investigated the expression of NE1 and NE2 signatures in external datasets. First, we investigated the single-cell study by Dong et al. who profiled six mCRPC patients, including two tumours (patients 4 and 6) that were positive for AR and INSM1 on histology[22] (A). As expected, in both patients there were cells co-expressing *AR* and *ASCL1*, suggesting a transition state. In cells of Patient 4, where there were fewer amphicrine cells and lower *ASCL1* levels, with overexpression of NE2. In contrast, in Patient 6, cells with higher *ASCL1* had higher expression of NE1 than NE2. The observation was concordant with our hypothesis that NE1 and NE2 describe two NE subtypes with NE1 more linked with *ASCL1* expression, while NE2 is more linked with transitioning, and NE^{mixed} is the most differentiated state (A).

We also investigated the expression of these signatures in CRPC samples from Prostate Cancer Atlas[23] (B). NE1/NE2 ratios were higher in low AR samples, in both CRPC and NEPC samples, with the trend being strongest in NEPC samples. Similarly, NE1/NE2 ratios increased with *ASLC1* levels. This is consistent with NE1 showing its highest expression at end-stages of NEPC development (low/no AR and high *ASCL1*), while NE2 is higher during NE transitioning stage where both positive *AR* and *ASCL1* (lower than end-stage NE) was observed, consistent with emerging earlier in neuroendocrine development.

In the xenograft models developed by Living Tumour Lab[24] treated with testosterone (GSE41193), a subset develops androgen-independence, and one model developed NEPC (LTL-331) (C). The model that developed NEPC showed the highest NE1/NE2 ratio at baseline. This ratio subsequently decreases with androgen independence but is still the highest of all xenografts. This suggest that NE1 and NE2 are sensitive to detect NEPC transformation at early stages of disease development.

Supplementary Note 4
Correlation between cell type proportions inferred from snRNA data and from immunohistochemistry (IHC)

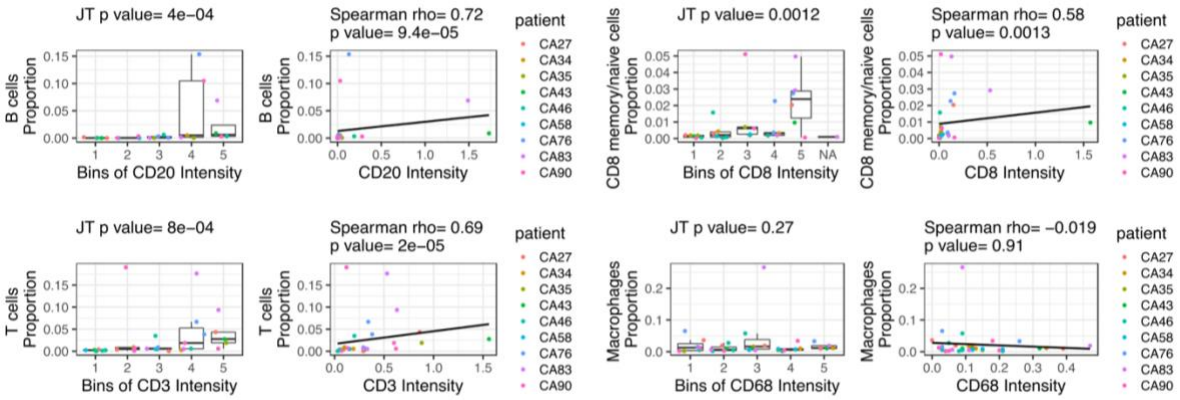

To validate the proportion of microenvironment cells in our data that were derived from the snRNAseq data, we performed staining of CD20, CD8, CD3 and CD68, to quantify B cells, CD8 T cells, T cells and macrophages on matched FFPE tissue sections. These show significant positive correlations, except between CD68 staining and macrophages. The IHC staining was done on slides of the same tissue samples as the fresh frozen samples used to generate the snRNAseq data. Therefore, complete matched cell composition was not expected. The Jonckheere-Terpstra (JT) and Spearman correlation tests were used to quantify the relationship between the IHC stain positive area proportion and the corresponding cell type proportion to the total cells of tissue.

Reference list for supplementary notes

1. Morgan, D. & Tergaonkar, V. Unraveling B cell trajectories at single cell resolution. *Trends Immunol.* **43**, 210–229 (2022).
2. Gómez Hernández, G., Morell, M. & Alarcón-Riquelme, M. E. The Role of BANK1 in B Cell Signaling and Disease. *Cells* **10**, 1184 (2021).
3. Szabo, P. A. *et al.* Single-cell transcriptomics of human T cells reveals tissue and activation signatures in health and disease. *Nat. Commun.* **10**, 4706 (2019).
4. Lendahl, U., Muhl, L. & Betsholtz, C. Identification, discrimination and heterogeneity of fibroblasts. *Nat. Commun.* **13**, 3409 (2022).
5. Single-cell analysis reveals prognostic fibroblast subpopulations linked to molecular and immunological subtypes of lung cancer | Nature Communications. https://www.nature.com/articles/s41467-023-35832-6.
6. Akil, A. *et al.* Notch Signaling in Vascular Endothelial Cells, Angiogenesis, and Tumor Progression: An Update and Prospective. *Front. Cell Dev. Biol.* **9**, (2021).
7. Lee, H. K., Chauhan, S. K., Kay, E. & Dana, R. Flt-1 regulates vascular endothelial cell migration via a protein tyrosine kinase-7–dependent pathway. *Blood* **117**, 5762–5771 (2011).
8. A Guide to Endothelial Cell Markers. https://www.biocompare.com/Editorial-Articles/598462-A-Guide-to-Endothelial-Cell-Markers/.
9. Kraus, D. M. *et al.* CSMD1 is a novel multiple domain complement-regulatory protein highly expressed in the central nervous system and epithelial tissues. *J. Immunol. Baltim. Md 1950* **176**, 4419–4430 (2006).
10. Pasman, J. A. *et al.* The CADM2 Gene and Behavior: A Phenome-Wide Scan in UK-Biobank. *Behav. Genet.* **52**, 306–314 (2022).
11. PubChem. KCNIP4 - potassium voltage-gated channel interacting protein 4 (human). https://pubchem.ncbi.nlm.nih.gov/gene/KCNIP4/human.
12. Tan, C. X. & Eroglu, C. Cell adhesion molecules regulating astrocyte-neuron interactions. *Curr. Opin. Neurobiol.* **69**, 170–177 (2021).
13. Zhang, H., Zhang, X., Xu, W. & Wang, J. TMC5 is Highly Expressed in Human Cancers and Corelates to Prognosis and Immune Cell Infiltration: A Comprehensive Bioinformatics Analysis. *Front. Mol. Biosci.* **8**, 810864 (2022).
14. Wang, L. *et al.* EHF promotes colorectal carcinoma progression by activating TGF-β1 transcription and canonical TGF-β signaling. *Cancer Sci.* **111**, 2310–2324 (2020).
15. Krzyzak, L. *et al.* CD83 Modulates B Cell Activation and Germinal Center Responses. *J. Immunol. Baltim. Md 1950* **196**, 3581–3594 (2016).
16. Luo, Y. *et al.* Single-cell transcriptomic analysis reveals disparate effector differentiation pathways in human Treg compartment. *Nat. Commun.* **12**, 3913 (2021).
17. Liu, L. *et al.* BCL-2 expression promotes immunosuppression in chronic lymphocytic leukemia by enhancing regulatory T cell differentiation and cytotoxic T cell exhaustion. *Mol. Cancer* **21**, 59 (2022).
18. Prasad, M. *et al.* Themis regulates metabolic signaling and effector functions in CD4+ T cells by controlling NFAT nuclear translocation. *Cell. Mol. Immunol.* **18**, 2249–2261 (2021).
19. Ma, R.-Y., Black, A. & Qian, B.-Z. Macrophage diversity in cancer revisited in the era of single-cell omics. *Trends Immunol.* **43**, 546–563 (2022).
20. Nguyen, Q. H. *et al.* Profiling human breast epithelial cells using single cell RNA sequencing identifies cell diversity. *Nat. Commun.* **9**, 2028 (2018).
21. Xie, T. *et al.* Single-Cell Deconvolution of Fibroblast Heterogeneity in Mouse Pulmonary Fibrosis. *Cell Rep.* **22**, 3625–3640 (2018).
22. Dong, B. *et al.* Single-cell analysis supports a luminal-neuroendocrine transdifferentiation in human prostate cancer. *Commun. Biol.* **3**, 1–15 (2020).
23. Bolis, M. *et al.* Dynamic prostate cancer transcriptome analysis delineates the trajectory to disease progression. *Nat. Commun.* **12**, 7033 (2021).
24. Lin, D. *et al.* High fidelity patient-derived xenografts for accelerating prostate cancer discovery and drug development. *Cancer Res.* **74**, 1272–1283 (2014).